23 June 2021

# Nitrene Photochemistry of Manganese N-Haloamides

Gerard Van Trieste[1], Madeline Hicks[1], Anuvab Das[1], Nattamai Bhuvanesh[1], Andrew Ozarowski[2], Joshua Telser[3], David Powers[1]

1. Texas A&M University
2. Florida State University
3. Roosevelt University

## Abstract

Here we report the synthesis and nitrene transfer photochemistry of Mn(III) N-haloamide complexes. Photolysis results in both C–H bond amination and olefinic aziridination products. Low-temperature spectroscopy indicates halogen-dependent photoreactivity: Photolysis of N-chloroamides cleaves the Mn–N bond to generate Mn(II) and amidyl radical species; in contrast, photolysis of N-iodoamides proceeds via N–I cleavage yielding a formally Mn(IV) nitrenoid.

## Keywords

Metal Nitrene, Photochemistry, C-H Amination, Reactive Intermediates

# Nitrene Photochemistry of Manganese *N*-Haloamides

Gerard P. Van Trieste III,[a] Madeline H. Hicks,[a] Anuvab Das,[a] Nattamai Bhuvanesh,[a] Andrew Ozarowski,[b] Joshua Telser,[c] and David C. Powers[a,*]

[a] Department of Chemistry, Texas A&M University, College Station, TX 77843, USA

[b] National High Magnetic Field Laboratory, Florida State University, Tallahassee, FL, 32310, USA

[c] Department of Biological, Physical and Chemical Sciences, Roosevelt University, Chicago, IL, 60605, USA

*powers@chem.tamu.edu

**Abstract** Manganese complexes supported by macrocyclic tetrapyrrole ligands represent an important platform for nitrene transfer catalysis and have been applied to both C–H amination and olefin aziridination catalysis. The reactivity of the transient high-valent Mn nitrenoids that mediate these processes renders characterization of these species challenging. Here we report the synthesis and nitrene transfer photochemistry of a family of Mn(III) *N*-haloamide complexes. The $S = 2$ *N*-haloamide complexes are characterized by $^1$H NMR, UV-vis, IR, high-frequency and -field EPR (HFEPR) spectroscopies, and single-crystal X-ray diffraction. Photolysis of these complexes results in the formal transfer of a nitrene equivalent to both C–H bonds, such as the a-C–H bonds of tetrahydrofuran, and olefinic substrates, such as styrene, to afford aminated and aziridinated products, respectively. Low-temperature spectroscopy and analysis of kinetic isotope effects for C–H amination indicate halogen-dependent photoreactivity: Photolysis of *N*-chloroamides proceeds via initial cleavage of the Mn–N bond to generate Mn(II) and amidyl radical intermediates; in contrast, photolysis of *N*-iodoamides proceeds via N–I cleavage to generate a Mn(IV) nitrenoid (*i.e.*, $\{MnNR\}^7$ species). These results establish *N*-haloamide ligands as viable precursors in the photosynthesis of metal nitrenes and highlight the power of ligand design to provide access to reactive intermediates in group-transfer catalysis.

## Introduction

Since Breslow's seminal discovery of Mn porphyrin-catalyzed amination of cyclohexane, Mn tetrapyrroles have emerged as an important platform for nitrene transfer catalysis.[1] The combination of nitrene precursors, such as iminoiodinanes[1c, 2] or *N*-haloamides,[3] and Mn(III) porphyrin catalysts enables nitrene transfer to C–H bonds and olefinic substrates to afford amines and aziridines, respectively (Figure 1). Enantioselective nitrene transfer catalysis has been realized using $D_4$-symmetric chiral Mn porphyrin catalysts.[2c, 4] More recently, White *et al.* have developed related Mn(III) phthalocyanines as highly active catalysts for aliphatic C–H amination.[5] In analogy to metalloporphyrin-supported metal oxo intermediates in C–H hydroxylation catalysis, the developed nitrene transfer catalysis is proposed to proceed via the intermediacy of reactive high-valent Mn nitrenoids.[6]

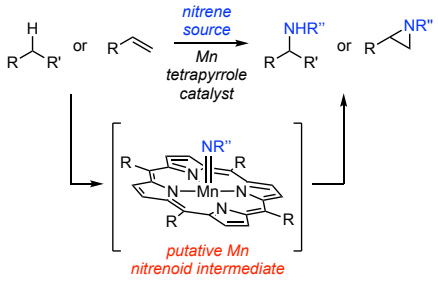


**Figure 1.** Mn tetrapyrrole-catalyzed nitrene transfer catalysis has been applied to both C–H amination and olefin aziridination reactions. Electrophilic Mn nitrenoids are proposed to mediate this family of nitrene transfer reactions.

The reactivity of the Mn nitrenoids that are invoked as transient intermediates in nitrene transfer catalysis renders these species challenging to observe.[7] Stabilization of these intermediates via synthetic modification of the ancillary ligand set can attenuate the reactivity of the supported Mn nitrenoid and enable isolation. Abu-Omar and co-workers leveraged triply anionic corrole ligands to stabilize and isolate Mn(V) nitrenoid **1**, which was prepared by photolysis of a solution of mesityl azide and Mn(III) *tris*-pentafluorophenylcorrole (Figure 2a).[8]

Complex **1** was found to be unreactive towards alkenes and alkanes but did participate in reaction with $PPh_3$ to afford the corresponding iminophospine. Goldberg and co-workers reported the isolation of corrolazine-supported nitrenoid **2**, which was similarly found to be unreactive towards either olefins or C–H bonds (Figure 2b).[9] Use of a tetraanionic tetraamido macrocyclic ligand (TAML) enabled the isolation of Mn(V) imido complex **3** (Figure 2c).[10] Further oxidation to the corresponding Mn(VI) complex was necessary to engender nitrene transfer chemistry. In the context of porphyrin-supported nitrenoids, acylation of Mn(V) nitrido complex **4** with trifluoroacetic anhydride affords Mn(V) nitrenoid **5**, which was characterized by $^1$H NMR and UV-vis spectroscopies and displays olefin aziridination activity (Figure 2d).[6d, 11]

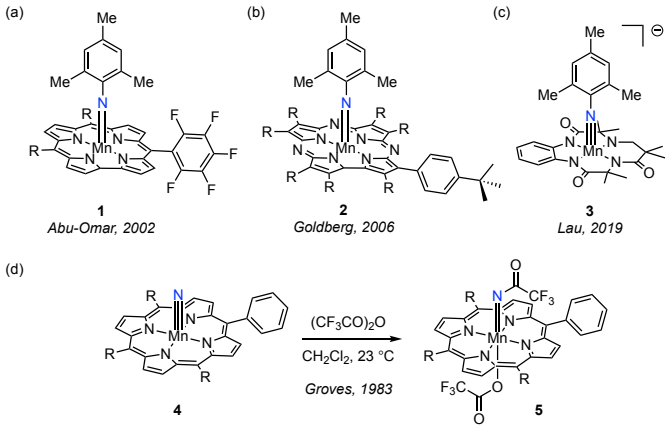


**Figure 2.** A small family of Mn(V) nitrenoids has been characterized, including (a) corrole-supported **1**, (b) corrolazine-supported **2**, and (c) TAML-supported **3**. (d) Treatment of Mn(V) nitride **4** with trifluoroacetic anhydride resulted in the observation of porphyrin-supported Mn(V) nitrenoid **5**.

Synthetic photochemistry provides opportunities to access reactive species under conditions that allow for characterization by time-resolved or cryogenic methods without necessitating stabilization via synthetic derivatization. In the context of Mn oxo chemistry, Newcomb and co-workers demonstrated that both Mn(IV) and Mn(V) oxo complexes could be accessed by photolysis of Mn oxyanion complexes (Figure 3a).[12] Flash photolysis of Mn(III)

chlorate complex **6a** resulted in Cl–O bond homolysis to generate a Mn(IV) oxo compound **7**; in contrast, flash photolysis of Mn(III) perchlorate complex **6b** resulted in Cl–O bond heterolysis to generate a Mn(V) oxo complex **8**. Similar photochemically promoted O–X cleavage to generate Mn oxo complexes was described by Suslick and co-workers in the context of porphyrin-supported Mn nitrite and nitrate complexes,[13] and Zhang and co-workers have described photogeneration of Mn oxo complexes from μ-oxo dimanganese precursors.[14]

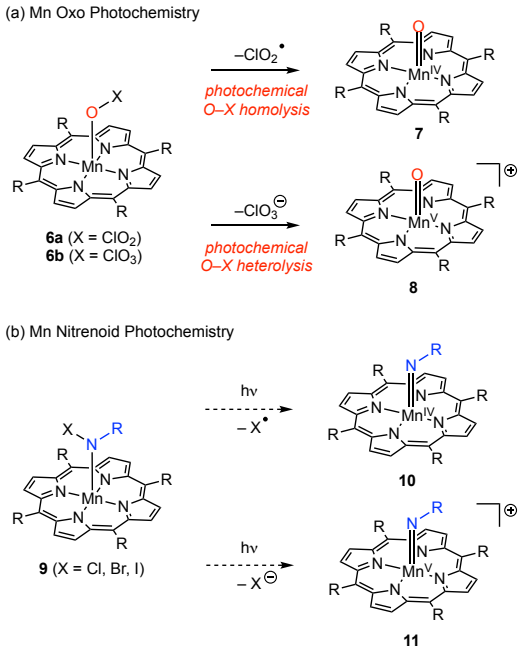


**Figure 3.** (a) Photolysis of Mn chlorate **6a** affords Mn(IV) oxo **7** via Cl–O homolysis whereas photolysis of Mn perchlorate **6b** affords Mn(V) oxo **7** via Cl–O homolysis. (b) Corresponding Mn nitrenoid photochemistry would be enabled if control over hetero- and homolytic N–X cleavage processes could be achieved in haloamide complexes.

In contrast to metal oxo chemistry, photochemical strategies to generate the corresponding reactive metal nitrenoids are much less developed. While organic azide ligands can represent viable photoprecursors to metal nitrenes, the poor donicity of organic azides as ligands coupled with the thermal instability of these ligands towards $N_2$ loss results in a limited family of potential photoprecursors.[15] Conceptually, haloamide ligands, which are X-type donors, could serve as

nitrene precursors via N–X photoactivation. In analogy to oxyanion photochemistry pictured in Figure 3a, both N–X homolysis and heterolysis mechanisms are potentially available to haloamide complexes (Figure 3b). In 2018, we demonstrated that photolysis of a $Rh_2$ complex with an *N*-chloroamide ligand afforded the corresponding $Rh_2$ nitrenoid via N–Cl homolysis.[16] Exploration of the generality of N–X photocleavage and the photoactivation modes available to a more diverse set of transition metal complexes is critical to generalizing *N*-haloamide photochemistry as an approach to catalytically relevant metal nitrenoids. At present, the synthetic chemistry of transition metal haloamide complexes is extremely limited, with only three structures reported,[16-17] and while significant work has been carried out on the photolysis of organic *N*-haloamines,[18] the corresponding photochemistry of inorganic *N*-haloamides is almost completely unknown.

Here we report the synthesis and characterization of a family of Mn porphyrins featuring *N*-haloamide ligands. These complexes are $S = 2$ species and are fully characterized in both solution phase and the solid state. This family of complexes includes the first examples of *N*-bromoamide and *N*-iodoamide complexes of transition metals. Photolysis of these complexes gives rise to the product of C–H amination and olefin aziridination. A combination of kinetic isotope effect analysis and low-temperature spectroscopy indicates that while the photolysis of Mn(III) *N*-chloroamides proceeds via initial cleavage of the Mn–N bond to generate Mn(II) and amidyl radical intermediates, photolysis of the corresponding *N*-iodoamide complexes proceeds via N–I cleavage to generate a Mn(IV) nitrenoid that participates in both C–H amination and olefin aziridination. These observations represent the first example of a porphyrin-supported Mn(IV) nitrenoid, highlight the impact of ligand design in the synthesis of novel photoprecursor ligands, and establish *N*-haloamides as a class of nitrene photoprecursor ligands.

## Results

***Synthesis and Characterization.*** Sequential treatment of porphyrin-supported Mn(III) chlorides **12** with $AgBF_4$ and M[NTsX] (M = Na or K; i.e., haloamine-T) provided access to the corresponding Mn(III) haloamide complex **13** (Figure 4; for characterization of the intermediate $[MnL]BF_4$ complexes, see Supporting Information). The spectroscopic data for iodoamide **13e** is representative of the family of haloamides and is described in detail here; for characterization details of the other haloamide complexes, see the Supporting Information. The $^1H$ NMR spectrum of **13e** displays three paramagnetically shifted peaks, which integrate as expected for the assigned structure (Figure S1). The UV-vis spectrum of **13e** displays absorbances at 383 nm ($\varepsilon = 3.5 \times 10^4$ $M^{-1}cm^{-1}$), 479 nm ($\varepsilon = 5.2 \times 10^4$ $M^{-1}cm^{-1}$), 585 nm ($\varepsilon = 7.8 \times 10^3$ $M^{-1}cm^{-1}$), and 620 nm ($\varepsilon = 8.2 \times 10^3$ $M^{-1}cm^{-1}$), which we assign as ligand-to-metal charge-transfer (LMCT), Soret, and Q-bands respectively, based on comparison to other Mn(III) porphyins.[12b] Based on the ratio of the molar absorptivities of the two Q-bands and the position of the Soret band, the ligand field strength of the N-iodoamide ligand is similar to that of chloride (*i.e.*, Mn(TPP)Cl) and the ligand field strength of the haloamide ligands examined here is not sensitive to the identity of the *N*-halogen (Table S1).[19]

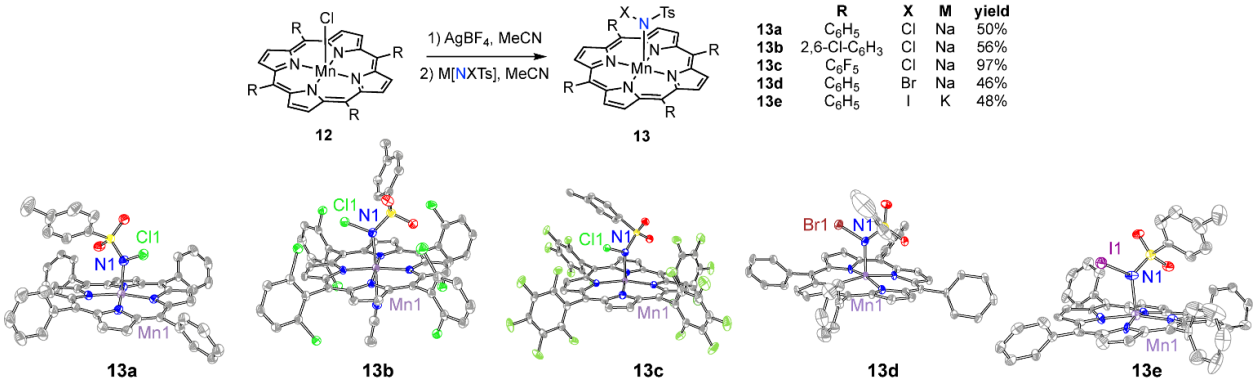


| | R | X | M | yield |
|---|---|---|---|---|
| **13a** | $C_6H_5$ | Cl | Na | 50% |
| **13b** | 2,6-Cl-$C_6H_3$ | Cl | Na | 56% |
| **13c** | $C_6F_5$ | Cl | Na | 97% |
| **13d** | $C_6H_5$ | Br | Na | 46% |
| **13e** | $C_6H_5$ | I | K | 48% |

**Figure 4.** Top: General synthetic strategy for the Mn(III) *N*-haloamide complexes **13**. Bottom: Displacement ellipsoid plots of the Mn *N*-haloamides **13**. H-atoms and solvent molecules have been omitted for clarity. Ellipsoids drawn at 50% probability.

Consistent with the $S = 2$ ground state typical of Mn(III) porphyrin complexes, compound **13e** displays a magnetic moment of 4.9 (Evans method, 23 °C) and does not display X-band EPR features at 4 K (2-Me-THF glass).[19a, 20] Due to the lack of X-band EPR features for $S = 2$ compounds, we pursued high-frequency and -field EPR (HFEPR) spectroscopic characterization of this suite of complexes (for spectra and resonance field versus microwave frequency plots of **13a**, **13d**, and **13e** see Figures S4-S10). The spectra consist of very broad signals apparently due to the presence of slightly different Mn moieties (two in **13a**, **13d**, and **13e**). Representative HFEPR spectra recorded at 319 GHz of the MnNXTs(TPP) X = Cl, Br, I series are illustrated in Figure 5 and the derived spin Hamiltonian parameters (zero field splitting (ZFS): axial ($D$), rhombic ($E$) values, and $g$ values) are collected in Table 1.[21] The present study is the first, to our knowledge, to provide the ZFS parameters of a Mn(III) tetrapyrrole with a nitrogen-donor axial ligand. The $D$ values of the compounds measured here are similar to each other and to other Mn(III) tetrapyrroles (*i.e.*, $D = -2.5 \pm 0.5$ cm$^{-1}$) bearing *O*- or *N*-bound axial ligands.[20, 22] Substitution of the amido halogen substituent has minimal impact on the $D$ value, with $D$ becoming slightly less negative from **13a** to **13d** to **13e**. This trend is significantly more dramatic in the corresponding MnX(TPP) series in which the halogen is bound directly to the Mn center.[23] This observation is a consequence of the extensive spin-orbit coupling of heavier donors.[24] The rhombicity does show a more significant dependence on the halogen identity, where **13a** is the least rhombic and **13e** is the most. We hypothesize that the high rhombicity value of MnNXTs(TPP) is due to the Ts–N–X apical unit breaking the four-fold symmetry observed in manganese tetrapyrroles, which generally feature rhombicity values close to zero, even in the case of corroles/corrolazines, which lack the true four-fold symmetry of the porphyrin macrocycle.[20, 22-23, 25] Qualitatively, Mn–N π-bonding from N $p_x$ (filled N lone pair) to Mn $d_{xz}$ (half-filled), but not correspondingly from N $p_y$ to Mn $d_{yz}$

would distinguish the in-plane *x* and y directions (the principal ZFS direction is along *z*, normal to the porphyrin plane).[20a]

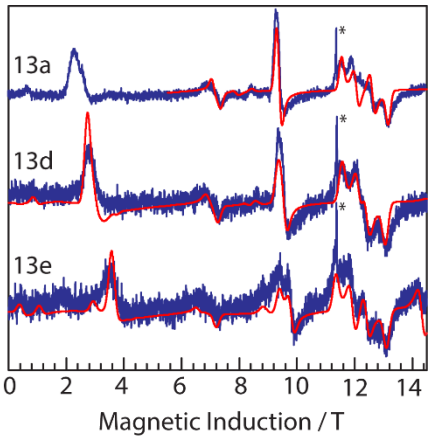


**Figure 5.** HF-EPR spectra of **13a**, **13d**, and **13e** collected at 319 GHz and 10 K. Blue: experimental; red: simulated with parameters given in Table 1. The asterisk indicates an impurity signal at g = 2.003.

**Table 1.** Comparison of HF-EPR data for compounds **13a**, **13d**, and **13e** with other axially coordinated Mn(III) tetrapyrrole analogues. *E* is given in the same sign as *D* (TPFC = 5,10,15-tris(pentafluorophenyl)corrole trianion; $TBP_8Cz$ = 2,3,7,8,12,13,17,18-octa(4-*tert*-butylphenyl)corrolazine).

| | $D$ / cm$^{-1}$ | $E$ / cm$^{-1}$ | $\lvert E/D \rvert$ | $g_x, g_y, g_z$ |
|---|---|---|---|---|
| **13a** | –2.881 | –0.095 | 0.033 | 1.994, 1.984, 1.979 |
| **13d** | –2.707 | –0.134 | 0.050 | 1.990, 1.995, 1.990 |
| **13e** | –2.460 | –0.243 | 0.099 | 2.004, 1.990, 1.991 |
| Mn(TPP)Cl[55-56] | –2.290 | ~0 | 0 | 1.98, 1.98, 2.00 |
| Mn(TPP)Br·$CDCl_3$[57] | –1.091 | –0.087 | 0.080 | 1.996, 1.985, 1.994 |
| Mn(TPP)I·$CDCl_3$[57] | 1.30 | 0.010 | 0.008 | 1,965, 1.971, 1.930 |
| Mn(TPFC)($OPPh_3$)[58] | –2.69 | –0.030 | 0.011 | 1.994, 1.994, 1.980 |
| Mn($TBP_8Cz$)(HOMe)[59] | –2.60 | –0.015 | 0.006 | 2.00 (isotropic) |

X-ray quality crystals of each of the Mn(III) haloamide complexes were obtained by cooling concentrated acetonitrile solutions to –35 °C; solid-state structures of **13** are collected in Figure 4 and relevant refinement data are collected in Tables S6-S10. The Mn(III) center in **13e** is five-coordinate. The Mn ion lies 0.271 Å above the $N_4$ plane, and the *N*-iodoamide ligand occupies one of the axial coordination sites. The haloamide nitrogen is approximately trigonal planar, with Mn–N–I = 119.1(3)°, Mn–N–S = 128.8(4)°, and S–N–I = 112.1(4)°. The bond metrics of **13a-d** are consistent with those described for **13e** with two exceptions: 1) the N–X bond length varies predictably as a function of halogen identity (*i.e.*, the N–Cl distance in **13a** is 1.745(3) Å, the N–

Br distance in **13d** is 1.884(6) Å, and the N–I distance in **13e** is 2.056(7) Å) and 2) the Mn center in **13b** is six-coordinate with an MeCN ligand in the final coordination site, which results in elongation of Mn–N(1) in **13b** (2.252(4) Å) as compared to **13a** (2.070(3) Å) or **13c** (2.1112(7) Å). Of note, complexes **13d** and **13e** are the first crystallographically characterized *N*-bromoamide and *N*-iodoamide complexes of a transition metal, respectively. For comparison of the metrical parameters of **13** with known chloroamides, see Table S13.

***Photolysis of Mn(III) Haloamides.*** Photolysis (λ > 335 nm) of an optically dilute solution of **13e** (4:1 MeCN:THF solution) affords Mn(II) complex **15**. UV-vis spectra collected periodically during the photolysis of a dilute solution of **13e** are characterized by well-anchored isosbestic points at 295, 408, 460, 514, 584, and 589 nm, which indicates the lack of steady state intermediates (Figure 6). The final spectrum overlays with that of Mn(II)TPP (**15**), which was independently prepared by treatment of **12** with $NaBH_4$ (Figure S11). ESI-MS analysis of the photolysis reaction mixture indicates the presence of sulfonamide **14**, the product of formal nitrene transfer to the a-C–H bond of THF. Preparative scale photolysis resulted in the isolation of sulfonamide **14** in 44% yield. The mass balance of the haloamide ligand is $TsNH_2$ (56% yield).

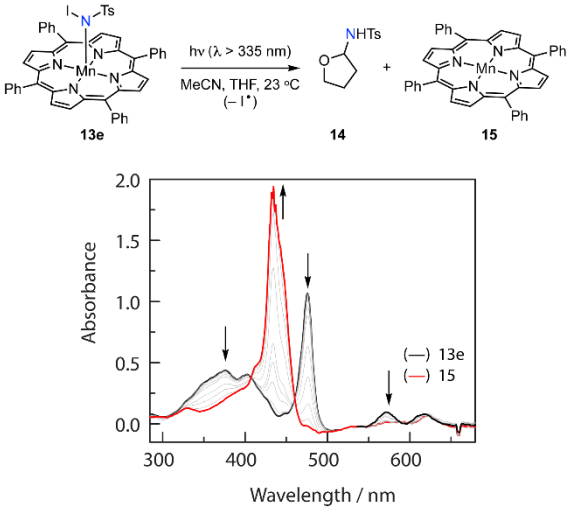


**Figure 6.** Photolysis (λ > 335 nm) of **13e** affords sulfonamide **14** and Mn(II) complex **15**. UV-vis spectra obtained periodically during the photolysis of **13e** display well-anchored isosbestic points at 295, 408, 460, 514, 584, and 589 nm, which indicate the lack of steady state intermediates during the conversion of **13e** to **15**.

The wavelength dependence of the observed photochemistry of **13e** was evaluated using 335 nm, 400 nm, and 495 nm long-pass filters. Only the 335 nm filter resulted in the spectral evolution illustrated in Figure 6a; no photoconversion was observed with a 400 or 495 nm long pass filter during the time scale of the experiment. However, prolonged photolysis (5 days) of **13e** with a 400 nm long pass filter yielded aminated THF (**14**) (40%, Table S2). These data are consistent with photochemistry arising from excitation of the LMCT band at 386 nm. Similar observations were reported by Suslick, that excitation of the analogous LMCT in Mn nitrate complexes was critical to accessing the corresponding Mn oxo complexes.[13b]

Complex **13e** participates in nitrene transfer photochemistry with a variety of substrates that are commonly encountered in Mn-catalyzed nitrene transfer chemistry (Figure 7). Photolysis of **13e** ($\lambda > 335$ nm) in a 4:1 MeCN:2-Me-THF solution results in sulfonamide **16** (19% yield), the product of formal nitrene insertion into the less hindered α-C–H bond. To probe the C–H bond strength requirement for amination, we examined the photochemical amination of toluene (C–H bond dissociation energy (BDE) = 89.7 kcal/mol[26]) and cyclohexane (C–H BDE = 99.5 kcal/mol[27]): Toluene underwent benzylic amination to afford compound **17** in 40% yield; cyclohexane did not participate in detectable amination chemistry. Photolysis of **13e** in the presence of styrene results in aziridine **18** in 30% yield. In all cases, the mass balance is accounted for by $TsNH_2$ and transfer of the NTs fragment requires photochemical activation: Thermolysis of **13e** in the presence of these substrates results in **15** and $TsNH_2$.

Haloamide complexes **13a**-**13d** also participate in photochemical amination of THF. Photolysis ($\lambda > 335$ nm) of a 4:1 MeCN:THF solution of **13a** afforded sulfonamide **14** in a 50% yield. Similar reactivity was observed for **13b**, **13c**, and **13d** (55, 70, and 63% yield of **14**,

respectively). In contrast to iodoamide **13e**, photolysis of **13a**-**13d** in the presence of either toluene or styrene does not result in the products of nitrene transfer.

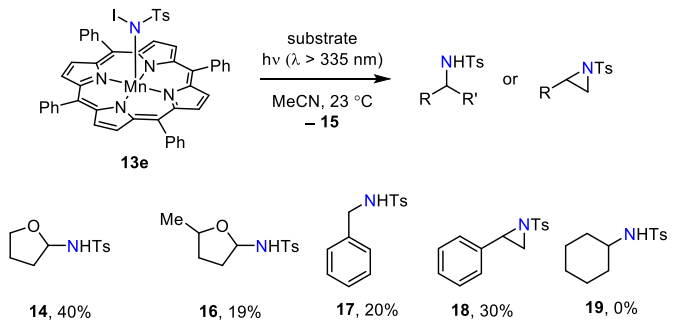


**Figure 7.** Nitrene transfer photochemistry of *N*-iodoamide complex **13e** with various C–H bonds and olefinic substrates. All yields are determined via $^1$H NMR with an internal standard of mesitylene. The formation of $TsNH_2$ accounts for the mass balance of nitrogen in these reactions.

***Determination of Kinetic Isotope Effects.*** To gain insight into the mechanism of C–H amination, we measured the deuterium kinetic isotope effect ($k_H/k_D$) for THF amination. Experimentally, solutions of photoprecursors 13 were photolyzed in a 1:1 solution of THF:THF-$d_8$ and the $k_H/k_D$ was determined by integration of the ESI-MS signals for **14** and **14**-$d_7$. Photolysis of a solution of **13e** at 23 °C afforded a $k_H/k_D$ = 18(3). For comparison, photolysis of **13a** in a 1:1 THF:THF-$d_8$ solution afforded a $k_H/k_D$ = 6(1).

***Cryogenic Photolysis.*** *Low Temperature Photolysis of* N-*Chloroamide* ***13a****.* To evaluate the primary photoproducts obtained from the described *N*-haloamides, we pursued low-temperature photolyses of these compounds in frozen solvent matrices. Photolysis of a 2-Me-THF glass of **13a** at 77 K resulted in the evolution of two new peaks in the UV-vis spectrum at 427 and 439 nm (Figure 8a). These peaks are well matched to spectral features of Mn(II) complex **15**, which could be generated by photoreduction of **13a** via Mn–N homolysis. To further confirm that the photolysis of **13a** generates Mn(II)(TPP), we measured the X-band EPR at 4K and 9.35 GHz following

irradiation of a 2-Me-THF glass of **13a** at 77K (Figure 8b). Mn(III) complex **13a** does not display an X-band EPR spectrum. Following photolysis, the measured spectrum exhibits features at $g_{\perp}$ = 6 and $g_{\|}$ = 2, which are consistent with those of independently prepared Mn(II) complex **15** and are as expected for an axial S = 5/2 system with D >> hv.[28] The differences in peak shape shown in Figure 8b are due to differential axial ligation. Compound **15** is formed via photocleavage of the Mn–N bond and thus has no axial ligand, whereas independently synthesized **15** has an axial THF ligand.[28b] The observed EPR features were insensitive to the photolysis matrix: Photolysis of a solvent-free thin film of **13a** resulted in the evolution of an EPR spectrum of **15** (Figure S14).

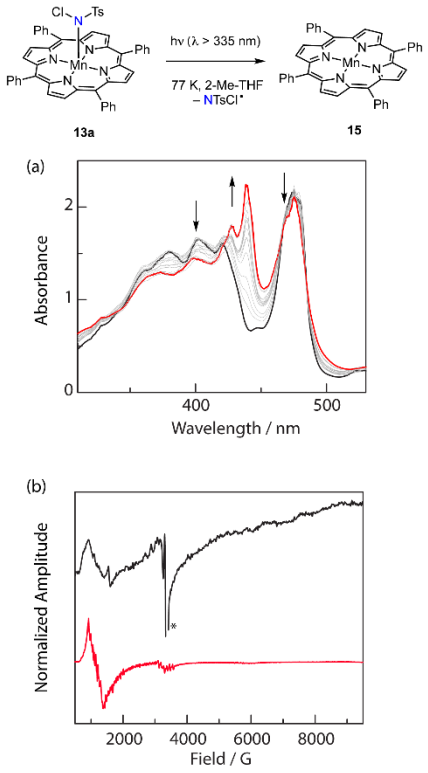


**Figure 8.** Low-temperature (77K) photolysis of Mn(TPP)(NClTs) (**13a**) results in photoreduction to generate Mn(II) complex **15**. (a) UV-vis spectra obtained periodically during the photolysis of **13a** at 77K display well-anchored isosbestic points at 295, 408, 460, 514, 584, and 589 nm. The peaks that grow in at 427 and 439 nm are attributed to Mn(II) complex **15** (a concentrated sample was utilized in this photolysis experiment, which resulted in detector saturation at 474 nm). (b) X-band EPR spectra following photolysis of **13a** (—) and of Mn(II)(TPP) (**15**) (—). *The peak at *g* = 2.0 has been truncated for clarity.

*Low Temperature Photolysis of* N-*Iodoamide* ***13e***. Photolysis of a 2-Me-THF glass of **13e** at 77K results in the evolution of a new peak in the UV-vis spectrum at 441 nm, which is distinct from the spectrum observed from photolysis of **13a** (Figure 9a). The X-band EPR spectrum of this sample measured at 4K and 9.35 GHz (Figure 9b) is significantly richer than that from the photolysis of **13a** (Figure 8b). Features across the entire field range are observed, corresponding to $g$ = 0.8, 1.2, 1.5, 2.0, 3.5, and 5.0. Such an EPR spectrum is inconsistent with either $S$ = 3/2 or 5/2 with $|D| >> h\nu$. Rather, it can be simulated as an $S$ = 5/2 complex with relatively small zfs ($|D|$ = 0.18 $cm^{-1}$ (5.4 GHz) and $|E|$ = 0.0037 $cm^{-1}$; $|E/D|$ = 0.020).[29] The spectral features of Mn(II) complex **15** are not observed in the spectrum obtained following photolysis of **13e**, nor are features expected of a potential Mn(IV) complex with simple X-type axial ligands.[30]

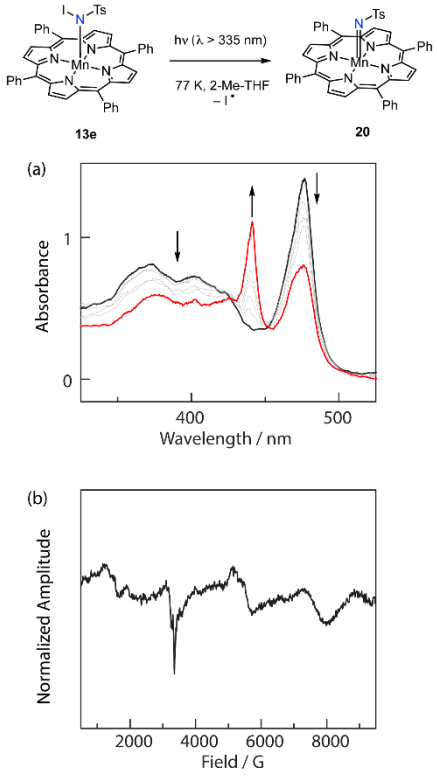


**Figure 9.** Low-temperature (77K) photolysis of Mn(TPP)(NITs) (**13e**) results in N–I cleavage to generate Mn(IV) nitrenoid complex **20**. (a) UV-vis spectra obtained periodically during the photolysis of **13e** at 77K display well-anchored isosbestic points at 429, 449, 511 nm. (b) X-band EPR spectra following photolysis of a 2-Me-THF glass of **13e** at 77K (—). This spectrum was simulated with parameters D = 0.18 $cm^{-1}$ and E = 0.0037 $cm^{-1}$ (—). *The peak at $g$ = 2.0 has been truncated for clarity.

Analysis of the temperature dependence of the EPR spectrum of **20** supports a high-spin configuration (*i.e.*, $S = 5/2$). Warming the sample from 4K to 77K results in the disappearance of the rich spectral features; only a signal at $g = 2.0$ which we hypothesize is from an organic radical generated in the photolysis. Subsequent re-cooling of the sample to 4K results in the reappearance of the spectral features illustrated in Figure 9b (Figure S15). These observations confirm that the loss of spectral features upon warming to 77K is due to spin-spin relaxation and not sample degradation.

Warming a sample of **20** generated in a 1 : 1 THF : THF-$d_8$ mixture at 77K to 23 °C affords amination product **14** with $k_H/k_D = 18$, which indicates that low-temperature and room-temperature photolyses generate the same reactive intermediate.

**Discussion**

Development of photochemical strategies to generate metal nitrenoid species promises to provide opportunities to study reactive intermediates that display fleeting lifetimes. Organic azide ligands have been recognized as potential photoprecursors to metal nitrenes, but few kinetically stable transition metal adducts of these ligands have been characterized.[15] We have been attracted to photoactivation of N–X bonds within haloamide ligands as a potentially generalizable strategy to photochemically generate nitrene fragments within the primary coordination sphere of transition metal ions. This strategy is motivated by the ubiquity of N–X photoactivation in the organic chemistry of haloamines[18] and by analogy to the oxo photochemistry of metal oxyanion complexes.[12-13] Unlike the organic chemistry of *N*-haloamines, however, the synthetic chemistry and photoactivity of *N*-haloamide complexes is almost completely undeveloped.

Application of *N*-haloamide ligands in nitrene photochemistry requires predictable and selective N–X activation chemistry. In the context of Mn(III) haloamide photochemistry, homolytic N–X bond cleavage would afford a Mn(IV) nitrenoid while heterolytic N–X bond activation would result in Mn(V) nitrenoids (Figure 10). In addition to these potential N–X activation modes, activation of the Mn–N bonds could give rise to Mn(II) and amidyl radicals.[13c, 31] Analogous O–X homolysis and heterolysis as well as M–O homolysis pathways have been documented in the oxo photochemistry of metal oxyanion complexes.[12-13]

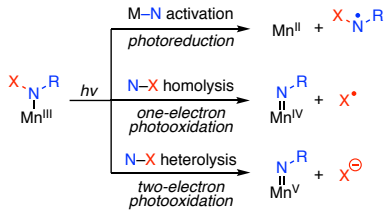


**Figure 10.** Summary of potential photoactivation pathways for Mn(III) *N*-haloamide complexes.

The Mn nitrenoid fragment in **20** is potentially redox non-innocent; thus the formal oxidation states of the Mn nitrenoids in the forgoing discussion are based on counting the nitrenoid fragment as a 2– ligand (*i.e.*, imido nomenclature). In the context of a formally Mn(IV) imido complex, *N*-centered non-innocence could result in a species more appropriately described as either a Mn(III) adduct of an iminyl radical anion ($RN^{\bullet-}$, $S = 1/2$) or as a Mn(II) adduct of a singlet nitrene ligand ($S = 0$). Applying the Enemark-Feltham nomenclature,[32] the Mn(IV) imide would be described as $\{MnNR\}^7$.

We have prepared a family of Mn(III) *N*-haloamides, Mn(TPP)(NXTs), as potential photoprecursors to reactive high-valent Mn nitrenoids relevant in Mn tetrapyrrole-catalyzed nitrene transfer (Figure 1). Solution-phase and solid-state characterization indicate the family of prepared complexes are $S = 2$ Mn(III) species. UV-vis spectroscopic measurements indicate that the donor strength of the *N*-haloamides is similar to that of chloride and is not meaningfully

impacted by the identity of the *N*-halogen atom. HFEPR indicates that the haloamide complexes are representative of Mn tetrapyrroles with light-atom axial donors, with enhanced rhombicity that may be due to anisotropic Mn–N π-bonding.

Photolysis of each of the prepared *N*-haloamide complexes in the presence of weak C–H bond donors, such as THF, results in formal nitrene transfer chemistry. Given previous demonstrations of C–H amination via amidyl radical intermediates,[33] the observation of amination products is insufficient to differentiate between the potential photogeneration of a high-valent nitrenoid or *N*-centered radical intermediates. Halogen-dependent photochemistry is observed with other substrates that are commonly encountered in nitrene transfer chemistry. Whereas *N*-chloroamide **13a** does not participate in photochemical aziridination of styrenes, *N*-iodoamide **13e** does undergo photochemical aziridination. These observations suggest that reactive nitrogen fragments generated from **13a** and **13e** differ; if both haloamides underwent similar photoactivation, one would expect that the resultant reactive species would display homologous substrate functionalization activity.

Analysis of the kinetic isotope effects for C–H functionalization demonstrates the decisive role of the halogen substituent on the resultant photochemistry and provides a direct reporter on the nature of the C–H cleavage event. Amination of THF by photolysis of *N*-chloroamide **13a** proceeds with $k_H/k_D$ = 6(1), which is consistent with values for H-atom abstraction reactions at *N*-centered radicals.[34] In contrast, amination of THF by photolysis of *N*-iodoamide **13e** proceeds with $k_H/k_D$ = 18(3). This large $k_H/k_D$ value exceeds the classical limit for H-atom transfer reactions between light atoms and is consistent with the large KIEs that are often encountered for amination via metal nitrenoids.[35]

Cryogenic photolysis provides both the opportunity to directly evaluate the course of the described photoreactions and evidence for the decisive impact of halogen identity on the resultant reactive nitrogen species. Both UV-vis and EPR spectroscopies indicate that the primary photoproduct obtained from chloroamide **13a** is Mn(II) complex **15**. The M–N homolysis that would generate complex **13** would also afford an amidyl radical intermediate, which would give rise to the observed amination products. In contrast, photolysis of iodoamide **13e** affords Mn(IV) nitrenoid **20**, the product expected of homolytic activation of the N–I bond of **13e**. Available data is consistent with the formation of an S = 5/2 species (*i.e.* an Mn(III) iminyl radical complex). The observed preference for Mn–N activation in **13a** and for N–I activation in **13e** is consistent with the relative N–Cl and N–I bond strengths and indicates the ability to control the course of the photoreaction by careful design of the photocleavable ligands.

## Conclusions

Synthesis and characterization of reactive intermediates capable of C–H functionalization reactions is central to the rational development of new selective and efficient catalysts. Synthetic photochemistry provides a platform to generate reactive intermediates under conditions in which they can be kinetically trapped, for example by providing a synthetic strategy to generate these species under cryogenic conditions. Application of synthetic photochemistry requires the availability of appropriate photoprecursor molecules and specifically access to photolabile ligands that exhibit predictable photoactivation modes. Here we have advanced *N*-haloamide ligands as a photolabile ligand in the synthesis of Mn nitrenoids. Isolation of homologous Mn(III) complexes featuring *N*-chloro-, *N*-bromo-, and *N*-iodoamide ligands provided the opportunity to observe the decisive impact of the halogen substituent on the observed photochemistry. Whereas the Mn(III)

chloroamide complex undergoes photoreduction via direct homolytic Mn–N activation, the corresponding Mn(III) iodoamide undergoes N–I activation to unveil a reactive Mn nitrenoid that participates in both C–H amination and olefin aziridination chemistry. A combination of low-temperature spectroscopy and analysis of C–H functionalization kinetic isotope effects indicates the critical photochemical difference between *N*-chloro- and *N*-iodoamide ligands. These observations mirror the competition between ligand-centered photoactivation chemistry and photoreduction reactions that are often encountered in the corresponding metal nitride and metal oxo photochemistries. The findings described here begin to delineate the design parameters needed to elicit ligand-centered bond activation to generate metal nitrenoids. We anticipate the development of general strategies in the synthetic photochemistry of metal nitrenoids will expand access to reactive nitrenoids relevant to catalysis, and we are actively working to expand the generality of the haloamide strategies described here.

**Author Contributions**

GPVT, AD, and DCP conceptualized the project. GPVT, MHH, AD, and AO carried out experimental work. All authors contributed to data analysis. DCP drafted the manuscript. All authors provided input to, and agreed with, the final manuscript.

**Acknowledgement**

The authors acknowledge the U.S. Department of Energy (DOE), Office of Science, Office of Basic Energy Sciences, Catalysis Program (DE-SC0018977), the Welch Foundation (A-1907), and an Alfred P. Sloan Fellowship to DCP for financial support. A portion of this work was performed at the National High Magnetic Field Laboratory, which is supported by NSF Cooperative Agreement DMR-1644779 and the State of Florida. Crystal structures of **13a**, **13b**, and **13c** were collected at NSF's ChemMatCARS Sector 15, which is principally supported by the Divisions of Chemistry (CHE) and Materials Research (DMR), NSF, under Grant NSF/CHE-1834750. Use of the Advanced Photon Source, an Office of Science User Facility operated for the U.S. Department of Energy (DOE) Office of Science by Argonne National Laboratory, was supported by the U.S. DOE under Contract DE-AC02-06CH11357.

## References


[1] a) R. Breslow, S. H. Gellman, *J. Chem. Soc., Chem. Commun.* **1982**, 1400–1401; b) S. Fantauzzi, A. Caselli, E. Gallo, *Dalton Trans.* **2009**, 5434–5443; c) C.-M. Che, V. K.-Y. Lo, C.-Y. Zhou, J.-S. Huang, *Chem. Soc. Rev.* **2011**, *40*, 1950–1975; d) Y. Park, Y. Kim, S. Chang, *Chem. Rev.* **2017**, *117*, 9247–9301; e) R. Singh, A. Mukherjee, *ACS Catal.* **2019**, *9*, 3604–3617; f) J. L. Jeffrey, R. Sarpong, *Chem. Sci.* **2013**, *4*, 4092–4106; g) W. Liu, L. Ackermann, *ACS Catal.* **2016**, *6*, 3743–3752; h) R. Breslow, S. H. Gellman, *J. Am. Chem. Soc.* **1983**, *105*, 6728–6729.

[2] a) J. Yang, R. Weinberg, R. Breslow, *Chem. Commun.* **2000**, 531–532; b) X.-Q. Yu, J.-S. Huang, X.-G. Zhou, C.-M. Che, *Org. Lett.* **2000**, *2*, 2233–2236; c) J.-L. Liang, J.-S. Huang, X.-Q. Yu, N. Zhu, C.-M. Che, *Chem. Eur. J.* **2002**, *8*, 1563–1572; d) J. P. Mahy, G. Bedi, P. Battioni, D. Mansuy, *Tetrahedron Lett.* **1988**, 1927–1930; e) J.-P. Mahy, G. Bedi, P. Battioni, D. Mansuy, *New. J. Chem.* **1989**, *3*, 651–657; f) D. Mansuy, J.-P. Mahy, A. Dureault, G. Bedi, P. Battioni, *J. Chem. Soc., Chem. Commun.* **1984**, 1161–1163.

[3] a) S. Cenini, A. Penoni, S. Tollari, *J. Mol. Catal. A: Chem.* **1997**, *124*, 109–113; b) R. Vyas, G.-Y. Gao, J. D. Harden, X. P. Zhang, *Org. Lett.* **2004**, 1907–1910.

[4] J.-P. Simonato, J. Pécaut, J.-C. Marchon, W. Robert Scheidt, *Chem. Commun.* **1999**, 989–990.

[5] a) J. R. Clark, K. Feng, A. Sookezian, M. C. White, *Nat. Chem.* **2018**, *10*, 583–591; b) S. M. Paradine, J. R. Griffin, J. Zhao, A. L. Petronico, S. M. Miller, M. Christina White, *Nat. Chem.* **2015**, *7*, 987–994.

[6] a) J. Wang, K. Zheng, T. Li, X. Zhan, *Catalysts* **2020**, *10*, 292; b) Z. Liu, Y. Lu, J. Guo, W. Hu, Y. Dang, Z.-X. Wang, *Org. Lett.* **2020**, *22*, 453–457; c) P. Li, Z. Cao, *Organometallics* **2019**, *38*, 343–350; d) J. T. Groves, T. Takahashi, *J. Am. Chem. Soc.* **1983**, *105*, 2073–2074.

[7] The term nitrenoid is used to describe a M–NR fragment where the electronic structure is still ambiguous

[8] R. A. Eikey, S. I. Khan, M. M. Abu-Omar, *Angew. Chem. Int. Ed.* **2002**, *41*, 3591–3595.

[9] D. E. Lansky, J. R. Kosack, A. A. Narducci Sarjeant, D. P. Goldberg, *Inorg. Chem.* **2006**, *45*, 8477–8479.

[10] H. Shi, J. Xie, W. W. Y. Lam, W.-L. Man, C.-K. Mak, S.-M. Yiu, H. K. Lee, T.-C. Lau, *Chem. Eur. J.* **2019**, *25*, 12895–12899.

[11] L. A. Bottomley, F. L. Neely, *J. Am. Chem. Soc.* **1988**, *110*, 6748–6752.

[12] a) R. Zhang, M. Newcomb, *J. Am. Chem. Soc.* **2003**, *125*, 12418–12419; b) R. Zhang, J. H. Horner, M. Newcomb, *J. Am. Chem. Soc.* **2005**, *127*, 6573–6582; c) M. Newcomb, R. Zhang, Z. Pan, D. N. Harischandra, R. E. P. Chandrasena, J. H. Horner, E. Martinez, *Catalysis Today* **2006**, *117*, 98–104; d) R. Zhang, M. Newcomb, *Acc. Chem. Res.* **2008**, *41*, 468–477.

[13] a) K. S. Suslick, P. A. Watson, *New J. Chem* **1992**, *16*, 633–642; b) K. S. Suslick, R. A. Watson, *Inorg. Chem.* **1991**, *30*, 912–919; c) K. S. Suslick, J. F. Bautista, R. A. Watson, *J. Am. Chem. Soc.* **1991**, *113*, 6111–6114; d) S. Klaine, F. Bratcher, C. M. Winchester, R. Zhang, *J. Inorg. Biochem* **2020**, *204*, 110986; e) R. Zhang, D. N. Harischandra, M. Newcomb, *Chem. Eur. J.* **2005**, *11*, 5713–5720; f) W. K. Ka, F. L. Ngo, D. Ranburger, J. Malone, R. Zhang, *J. Inorg. Biochem.* **2016**, *163*, 39–44; g) N. F. Lee, J. Malone, H. Jeddi, K. W. Kwong, R. Zhang, *Inorg. Chem. Commun.* **2017**, *82*, 27–30.

[14] K. W. Kwong, C. M. Winchester, R. Zhang, *Inorg. Chim. Acta* **2016**, *451*, 202–206.

[15] a) A. Das, Y.-S. Chen, J. H. Reibenspies, D. C. Powers, *J. Am. Chem. Soc.* **2019**, *141*, 16232–16236; b) A. Das, C.-H. Wang, G. P. Van Trieste, C.-J. Sun, Y.-S. Chen, J. H. Reibenspies, D. C. Powers, *J. Am. Chem. Soc.* **2020**, *142*, 19862–19867; c) M. Goswami, V. Lyaskovskyy, S. R. Domingos, W. J. Buma, S. Woutersen, O. Troeppner, I. Ivanović-Burmazović, H. Lu, X. Cui, X. P. Zhang, E. J. Reijerse, S. DeBeer, M. M. van Schooneveld, F. F. Pfaff, K. Ray, B. de Bruin, *J. Am. Chem. Soc.* **2015**, *137*, 5468–5479; d) Z. Guo, X. Guan, J.-S. Huang, W.-M. Tsui, Z. Lin, C.-M. Che, *Chem. Eur. J.* **2013**, *19*, 11320–11331; e) Y. Liu, J. Wei, C.-M. Che, *Chem. Commun.* **2010**, *46*, 6926–6928.

[16] A. Das, A. G. Maher, J. Telser, D. C. Powers, *J. Am. Chem. Soc.* **2018**, *140*, 10412–10415.

[17] a) M. M. Olmstead, P. P. Power, *Inorg. Chem.* **1986**, *25*, 4057–4058; b) V. I. Shcherbakov, V. P. Kuznetsova, E. V. Chuprunov, T. I. Ovsetsina, N. E. Stolyarova, L. N. Zakharov, N. Novgorod, *Organomet. Chem. (USSR)* **1991**, *4*, 1350–1354.

[18] a) R. S. Neale, *Synthesis* **1971**, *1971*, 1–15; b) L. M. Stateman, K. M. Nakafuku, D. A. Nagib, *Synthesis* **2018**, *50*, 1569–1586; c) M. E. Wolff, *Chem. Rev.* **1963**, *63*, 55–64; d) S. Z. Zard, *Chem. Soc. Rev.* **2008**, *37*, 1603–1618.

[19] a) L. J. Boucher, *Coord. Chem. Rev* **1972**, *7*, 289–329; b) L. Mu, J. Huang, Y. Zhou, P. Shen, *Polyhedron* **1997**, *16*, 2885–2888.

[20] a) J. Krzystek, J. Telser, L. A. Pardi, D. P. Goldberg, B. M. Hoffman, L.-C. Brunel, *Inorg. Chem.* **1999**, *38*, 6121–6129; b) J. Krzystek, A. Schnegg, A. Aliabadi, K. Holldack, S. A. Stoian, A. Ozarowski, S. D. Hicks,

M. M. Abu-Omar, K. E. Thomas, A. Ghosh, K. P. Caulfield, Z. J. Tonzetich, J. Telser, *Inorg. Chem.* **2020**, *59*, 1075–1090.
[21] Hˆ=μ_B B{g} Sˆ+D{Sˆ_z^2-1/3 S(S+1)}+E(Sˆ_x^2-Sˆ_y^2)
[22] a) J. Krzystek, L. A. Pardi, L.-C. Brunel, D. P. Goldberg, B. M. Hoffman, S. Licoccia, J. Telser, *Spectrochim. Acta, Part A* **2002**, *58*, 1113–1127; b) J. Krzystek, J. Telser, B. M. Hoffman, L.-C. Brunel, S. Licoccia, *J. Am. Chem. Soc.* **2001**, *123*, 7890–7897.
[23] A. N. Bone, S. E. Stavretis, J. Krzystek, Z. Liu, Q. Chen, Z. Gai, X. Wang, C. A. Steren, X. B. Powers, A. A. Podlesnyak, X.-T. Chen, J. Telser, H. Zhou, Z.-L. Xue, *Polyhedron* **2020**, *184*, 114488.
[24] S. Mossin, H. Weihe, A.-L. Barra, *J. Am. Chem. Soc.* **2002**, *124*, 8764–8765.
[25] a) D. E. Lansky, B. Mandimutsira, B. Ramdhanie, M. Clausén, J. Penner-Hahn, S. A. Zvyagin, J. Telser, J. Krzystek, R. Zhan, Z. Ou, K. M. Kadish, L. Zakharov, A. L. Rheingold, D. P. Goldberg, *Inorg. Chem.* **2005**, *44*, 4485–4498; b) J. Bendix, H. B. Gray, G. Golubkov, Z. Gross, *Chem. Commun.* **2000**, 1957–1958.
[26] S. J. Blanksby, G. B. Ellison, *Acc. Chem. Res.* **2003**, *36*, 255–263.
[27] Y.-R. Luo, *Handbook of Bond Dissociation Energies in Organic Compounds*, CRC Press, Boca Raton, **2002**.
[28] a) T. Jin, T. Suzuki, T. Imamura, M. Fujimoto, *Inorg. Chem.* **1987**, *26*, 1280–1285; b) S. Konishi, M. Hoshino, M. Imamura, *J. Phys. Chem.* **1982**, *86*, 1412–1414.
[29] The observed features are approximately consistent with the simulation provided with these parameters. A number of simulations with other parameters provide similar agreement with the experimental data and additional investigation, like a HFEPR study, is needed to unambiguously resolve the problem.
[30] M. J. Camenzind, F. J. Hollander, C. L. Hill, *Inorg. Chem.* **1983**, *22*, 3776–3784.
[31] a) M. Yamaji, Y. Hama, Y. Miyazaki, M. Hoshino, *Inorg. Chem.* **1992**, *31*, 932–934; b) M. Hoshino, Y. Nagashima, H. Seki, M. De Leo, P. C. Ford, *Inorg. Chem.* **1998**, *37*, 2464–2469.
[32] J. H. Enemark, R. D. Feltham, *Coord. Chem. Rev* **1974**, *13*, 339–406.
[33] a) A. S. Nazran, D. Griller, *J. Am. Chem. Soc.* **1983**, *105*, 1970–1971; b) J. Davies, T. D. Svejstrup, D. Fernandez Reina, N. S. Sheikh, D. Leonori, *J. Am. Chem. Soc.* **2016**, *138*, 8092–8095; c) M. D. Kärkäs, *ACS Catal.* **2017**, *7*, 4999–5022.
[34] C. Martínez, K. Muñiz, *Angew. Chem. Int. Ed.* **2015**, *54*, 8287–8291.
[35] a) Y. Dong, R. M. Clarke, G. J. Porter, T. A. Betley, *J. Am. Chem. Soc.* **2020**, *142*, 10996–11005; b) Y. Baek, T. A. Betley, *J. Am. Chem. Soc.* **2019**, *141*, 7797–7806; c) M. J. T. Wilding, D. A. Iovan, T. A. Betley, *J. Am. Chem. Soc.* **2017**, *139*, 12043–12049; d) E. R. King, E. T. Hennessy, T. A. Betley, *J. Am. Chem. Soc.* **2011**, *133*, 4917–4923; e) S.-M. Au, J.-S. Huang, W.-Y. Yu, W.-H. Fung, C.-M. Che, *J. Am. Chem. Soc.* **1999**, *121*, 9120–9132; f) Y. M. Badiei, A. Dinescu, X. Dai, R. M. Palomino, F. W. Heinemann, T. R. Cundari, T. H. Warren, *Angew. Chem. Int. Ed.* **2008**, *47*, 9961–9964; g) L. M. Slaughter, P. T. Wolczanski, T. R. Klinckman, T. R. Cundari, *J. Am. Chem. Soc.* **2000**, *122*, 7953–7975.